

# From Layered Zeolite Precursors to Zeolites with a Three-Dimensional Porosity: Textural and Structural Modifications through Alkaline Treatment

Trees De Baerdemaeker,<sup>†</sup> Mathias Feyen,<sup>‡</sup> Thomas Vanbergen,<sup>†</sup> Ulrich Müller,<sup>‡</sup> Bilge Yilmaz,<sup>§</sup> Feng-Shou Xiao,<sup>#</sup> Weiping Zhang,<sup>⊥</sup> Toshiyuki Yokoi,<sup>||</sup> Xinhe Bao,<sup>⊗</sup> Dirk E. De Vos,<sup>\*,†</sup> and Hermann Gies<sup>▽</sup>

<sup>†</sup>Centre for Surface Chemistry and Catalysis, KU Leuven, 3001 Leuven, Belgium

<sup>‡</sup>Chemicals Research and Engineering, BASF SE, 67056 Ludwigshafen, Germany

<sup>§</sup>Chemicals Research and Engineering, BASF Corporation, Iselin, New Jersey 08830, United States

<sup>#</sup>Zhejiang University, 310028 Hangzhou, China

<sup>⊥</sup>State Key Laboratory of Fine Chemicals, Dalian University of Technology, 116024 Dalian, China

<sup>||</sup>Chemical Resources Laboratory, Tokyo Institute of Technology, 226-8503 Yokohama, Japan

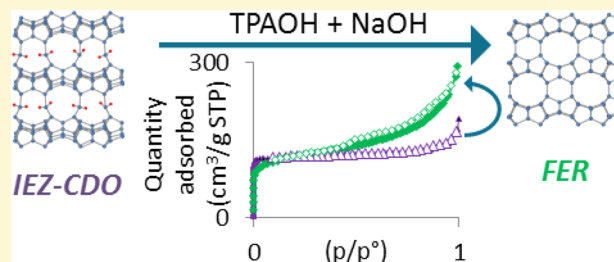
<sup>⊗</sup>State Key Laboratory of Catalysis, Dalian Institute of Chemical Physics, 116023 Dalian, China

<sup>▽</sup>Institute of Geology, Mineralogy and Geophysics, Ruhr-University Bochum, 44780 Bochum, Germany

## Supporting Information

**ABSTRACT:** The layered zeolite precursor RUB-36, consisting of ferrierite-type layers, can be transformed into a three-dimensional framework through various methods such as topotactic condensation into the CDO topology, or interlayer expansion either in the presence or absence of a silylating agent. However, the plate-like morphology of the micrometer sized crystals hampers the accessibility of the 2D micropore system, in which the channels run parallel to the plates. With the aim of introducing mesoporosity, alkaline treatments were performed on different RUB-36 derived expanded materials, and on RUB-36

itself. The effect on the physicochemical properties was examined using N<sub>2</sub> physisorption, powder X-ray diffraction, scanning electron microscopy and <sup>27</sup>Al MAS NMR whereas the influence on the catalytic activity was evaluated using esterification and alkylation reactions. After calcination, the purely inorganic, interlayer expanded material could be transformed into a mesopore containing FER-type material by selective removal of the interlayer T atom followed by the recombination of the layers. In the precalcination state, organic moieties, originating from the silylating agent or from the organic structure directing agent (OSDA), increase the hydrophobicity of the interlayer expanded structure and its stability against the alkaline treatment. In RUB-36, the high OSDA content limited the amount of mesopore formation through alkaline treatment. However, using the appropriate conditions, the subsequent interlayer expansion of alkaline treated RUB-36 also resulted in a mesopore containing interlayer expanded structure.



## INTRODUCTION

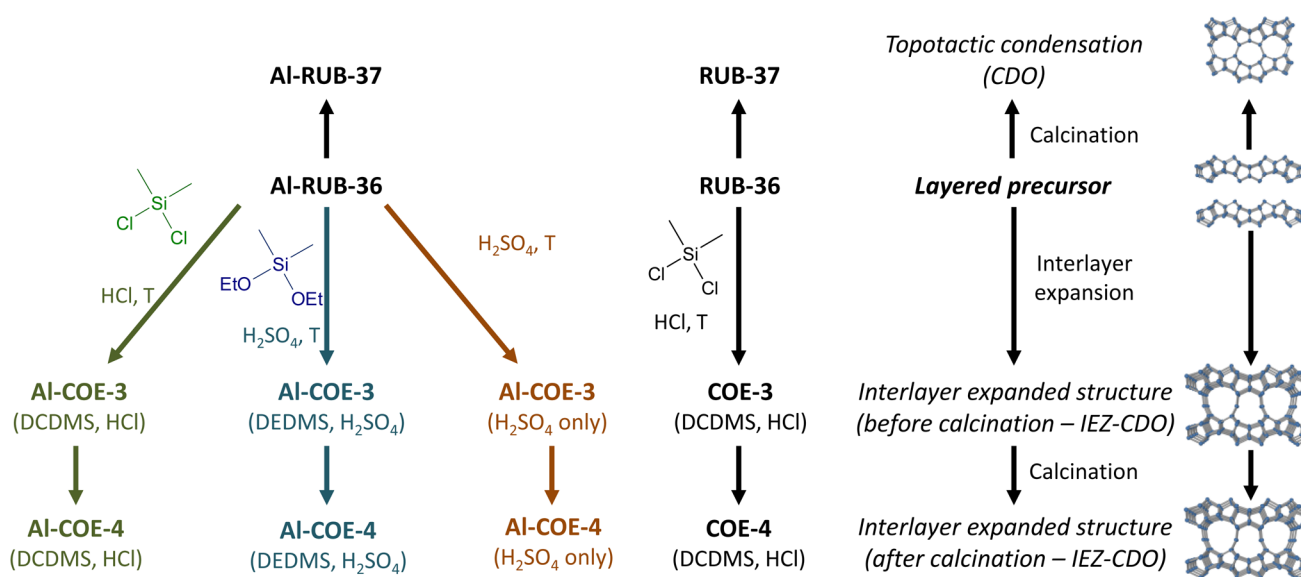
Zeolites are a well-known class of crystalline, microporous materials, which are widely used as catalysts, adsorbents and ion-exchangers.<sup>1</sup> Because of their well-defined, uniform pore system, they show remarkable shape-selective properties in chemical transformations.<sup>2,3</sup> The close relationship between the particular pore system of a zeolite and its catalytic properties continuously stimulates the search for new zeolite structures. One of the strategies in developing these new materials is based on the transformation of layered zeolite precursors into new zeolite topologies and other catalytically active materials. This topic has received much attention over the past two decades. Three-dimensional zeolites for which a layered precursor has

been identified include materials with AST, CAS, CDO, FER, MTF, MWW, NSI, PCR, RRO, RWR and SOD topologies as well as zeolite SSZ-81 with an unknown structure.<sup>4–18</sup> The layered zeolite precursors are typically obtained as products from hydrothermal synthesis. However, 3D zeolites can also be transformed into a 2D layered zeolite precursor. Typical examples are the germanosilicates with UTL or IWW topology of which the structure contains double four-rings preferentially occupied by Ge. The easy hydrolysis of the Ge–O bonds allows

Received: October 30, 2014

Revised: December 15, 2014

Published: December 17, 2014

Scheme 1. Overview of the Synthesis Strategies and Nomenclature of the Investigated RUB-36 based Materials<sup>a</sup>

<sup>a</sup>Al-containing or purely siliceous.

for selective extraction of Ge from the framework, which, depending on topology, Ge-content and treatment conditions, can result in a layered zeolite precursor,<sup>17,18</sup> in new frameworks through alternative connections of the layers found in the parent structure,<sup>14,19,20</sup> or in a material with the preserved, original topology but with a lower Ge content.<sup>21,22</sup>

Zeolite precursor layers can be considered as versatile building blocks for the synthesis of new materials. For instance, their topotactic condensation results in a corresponding three-dimensional zeolite with a topology, which cannot always be obtained through direct synthesis, as illustrated by the synthesis of RUB-41 (RRO topology) from the layered silicate RUB-39.<sup>9</sup> Other types of modification include the swelling and delamination of the layers,<sup>23</sup> pillarizing, during which the layers are swollen and subsequently stabilized by blocks of amorphous silica,<sup>24</sup> recombination, in which the layers are allowed to shift relative to one another<sup>25</sup> and interlayer expansion by the insertion of an additional T atom in between the precursor layers in order to create a new pore system.<sup>26</sup> In this last modification treatment, the layered precursor is treated with an acid solution at elevated temperatures which allows for the extraction of the organic structure directing agent (OSDA) from between the layers and the concurrent insertion of the additional T atom. The source of the additional T atom is typically a silylating agent, such as dichlorodimethylsilane (DCDMS) or diethoxydimethylsilane (DEDMS), but in some cases, the source is simply silica debris, either still present in the layered precursor from unreacted synthesis gel or generated from the crystalline layers during harsh postsynthesis treatments.<sup>27</sup> Using this interlayer expansion strategy, a highly selective hydroisomerization catalyst was synthesized from Al-containing RUB-36.<sup>28</sup> A more detailed overview of the synthesis and modification possibilities of layered zeolite precursors and related materials is provided in several recent publications.<sup>29–31</sup> Moreover, a classification system providing a summary of the different materials derived from layered zeolite precursors and their relation to traditional 3D zeolites has been proposed.<sup>32</sup>

A common drawback of the different layered zeolite precursors is the combination of a plate-like morphology with relatively large crystals which can only be accessed from the rim of the crystal plates.<sup>33</sup> This most likely results in diffusional limitations and hampers the efficient use of the catalyst. One way of improving the accessibility of the active sites is indeed through the above-mentioned delamination and pillaring strategies, which have been shown to be useful for the conversion of bulky molecules.<sup>34</sup> However, in these cases, the active sites responsible for the conversion are located on the outer surface of the layers rather than within micropore channels. An interesting alternative strategy to improve the accessibility of large crystals is the introduction of a secondary (meso)pore system via selective leaching.<sup>35</sup> Although dealumination through steaming and/or acid leaching is a widely known strategy, the low amount of Al incorporated in many of the layered precursors would limit the extent to which mesoporosity can be introduced. Therefore, desilication through alkaline treatment seems a more appropriate approach. Over the past decade, considerable research effort has been directed toward the creation of hierarchical zeolites through desilication. Most of the work focused on MFI-type zeolites<sup>36–39</sup> but other topologies, such as \*BEA, CHA, DDR, FAU, FER, IFR, HEU, LTA, LTL, MOR, TON, TUN, MWW and MTW have also been investigated.<sup>40–50</sup> This thorough investigation of the alkaline treatment of zeolites has resulted in a number of insights. First of all, the Si/Al ratios of aluminosilicate zeolites typically decrease because of the selective leaching of Si from the framework. However, several authors have pointed out that Al is also initially removed but to a lesser extent.<sup>51,52</sup> Moreover, the leached Al has a tendency to adsorb onto the zeolite surface, hence protecting it from further leaching. In this way, Al and other trivalent (framework) atoms play a pore-directing role by preventing uncontrolled dissolution from the crystal edges while still allowing some leaching to take place. In the case of highly siliceous zeolites, Pérez-Ramírez and co-workers found that these trivalent atoms can be added during the alkaline treatment and still assume the same pore-directing role as framework Al species.<sup>53</sup> Similarly,

tetrapropylammonium ions ( $\text{TPA}^+$ ) have been found to mildly adsorb to the zeolite surface and exert a comparable pore-directing role as Al. The concentration of these pore-directing agents is crucial, as too high concentrations result in complete surface coverage preventing selective extraction while too low concentrations can result in unselective zeolite dissolution. Furthermore, the presence of OSDA in the zeolite pores protects the structure against alkaline leaching.<sup>38</sup> Finally, the type of zeolite framework, the crystal morphology and the presence of defects also influence the effectiveness of mesopore formation.<sup>39,40</sup>

In this contribution, we subject materials derived from the layered precursor RUB-36 to an alkaline treatment to investigate the effect on their physicochemical and catalytic properties. RUB-36 consists of the ferrierite-type layer and can be transformed into the three-dimensional zeolite RUB-37 (CDO topology) through topotactic condensation, or into COE-4 (interlayer expanded zeolite, topology hereafter indicated with IEZ-CDO) after interlayer expansion and subsequent calcination.<sup>54</sup> An overview of the synthesis strategy of the different materials investigated in this contribution is shown in Scheme 1. Different treatment conditions were applied to investigate the effect on the textural properties and structure of the material. The effect of the treatment on the catalytic properties was investigated by comparing the performance of the alkaline treated catalysts to that of their untreated counterparts in acid-catalyzed esterification and alkylation reactions.

## ■ EXPERIMENTAL SECTION

**Catalyst Synthesis.** RUB-36. According to the previously published procedure,<sup>28</sup> Al-containing RUB-36 (Al-RUB-36) was synthesized using an aluminosilicate gel with diethyldimethylammonium hydroxide (DEDMAOH) as an organic structure directing agent (OSDA) and a molar ratio of  $\text{SiO}_2$ :0.005  $\text{Al}_2\text{O}_3$ :0.5 OSDA:10  $\text{H}_2\text{O}$ . The Si/Al ratio of the obtained material was 102, indicating nearly complete Al incorporation. For comparison, Al-free RUB-36 was also synthesized using an analogous procedure and synthesis gel.

RUB-37. The topotactic condensation of RUB-36 to RUB-37 was achieved via calcination in air at 600 °C for 4 h (heating rate 1 °C/min).

**Interlayer expansion of RUB-36.** Interlayer expansion of Al-RUB-36 results in Al-COE-3 type materials. Three types of interlayer expansion treatments were used. In a first experiment, Al-COE-3 was synthesized hydrothermally according to ref 21, using DCDMS as a bridging agent and HCl. For the Cl-free synthesis of Al-COE-3, DCDMS was replaced by DEDMS and HCl by  $\text{H}_2\text{SO}_4$ . A third type of COE-3 was obtained from an interlayer expansion treatment using only  $\text{H}_2\text{SO}_4$  (aq) without additional silylating agent. In this case, the interlayer expansion is accomplished by silica debris.<sup>27</sup>

Al-COE-4. Al-COE-4 type materials were obtained by calcination in air at 500 °C for 5 h (heating ramp 1 °C/min), starting with the respective COE-3 counterparts.

**Zeolite Modification. Alkaline Treatments.** Alkaline treatments were based on Verboekend and Pérez-Ramírez.<sup>53</sup> In a typical run, 200 mg of zeolite was added to a 10 mL crimp cap vial with a magnetic stirring rod. 6 mL of an alkaline solution was added, and the vial was placed in a heated copper block for a predetermined duration under stirring at 500 rpm. Afterward, the desilication was quenched on ice and the remaining solids were washed with water using centrifugation until the pH of the supernatant was neutral. Subsequently, the solids were dried overnight at 60 °C. Sources of alkalinity were sodium hydroxide, DEDMAOH and tetrapropylammonium hydroxide (TPAOH). Unless otherwise indicated, the desilications were performed at 65 °C for 0.5 h using a total base concentration of 0.2 M. For lower concentrations of TPAOH or DEDMAOH, NaOH was

used to adjust the total base concentration. Additional experiments using 0.4 M NaOH were also performed. The influence of  $\text{Al}(\text{OH})_4^-$  in the desilication suspension was investigated by adding an appropriate amount of  $\text{Al}(\text{NO}_3)_3 \cdot 9\text{H}_2\text{O}$ , resulting in 0.003–0.03 M  $\text{Al}(\text{OH})_4^-$  concentrations.

**Calcination and Ion-Exchange.** Prior to all physicochemical characterization and catalytic testing, the alkaline treated materials were first calcined in air at 500 °C for 5 h (heating rate 1 °C/min) to remove any residual organic material. To remove any remaining  $\text{Na}^+$  ions, the materials treated with NaOH were ion-exchanged three times using 0.5 M  $\text{NH}_4\text{NO}_3$  followed by calcination at 450 °C (5 h, heating rate 1 °C/min).

**Acid Treatment.** After desilication, some materials were subjected to a mild acid treatment to investigate the removal of extra-framework aluminum species. 0.1 g of zeolite was added to 3 mL aqueous 0.1 M HCl and treated at 70 °C for 6 h, followed by washing, and drying at 60 °C.

**Characterization.** Powder X-ray diffraction (XRD) patterns for zeolite structure confirmation were routinely collected on a STOE STADI P diffractometer equipped with an image plate detector using Cu  $\text{K}\alpha$  radiation and Debye–Scherrer geometry. XRD patterns of selected samples were additionally collected on a STOE STADI MP diffractometer in Debye–Scherrer geometry using a linear position sensitive detector (6°  $2\theta$  window), a Ge(111) monochromator (Cu  $\text{K}\alpha_1$  radiation,  $\lambda = 0.154056$  nm) and a capillary sample holder. Scanning electron microscopy (SEM) images were collected on a Philips XL30 SEM FEG microscope to investigate crystal morphology and size.<sup>27</sup> Al MAS NMR spectra of hydrated samples were collected on a Bruker DSX400 spectrometer ( $B_0 = 9.4$  T) accumulating 36 000 scans with a 0.30  $\mu\text{s}$  pulse and a 100 ms recycle delay. The spinning frequency of the 2.5 mm zirconia rotor was 20 kHz and a 0.1 M aqueous  $\text{Al}(\text{NO}_3)_3 \cdot 9\text{H}_2\text{O}$  solution was used as chemical shift reference. Thermogravimetric analysis (TGA) of the hydrated samples was performed on a TGA Q500 (TA Instruments) by heating approximately 10 mg of the sample from room temperature to 800 °C at 10 °C/min under  $\text{O}_2$  flow ( $\text{O}_2/\text{N}_2$  9). Textural characteristics of the samples were investigated by collecting  $\text{N}_2$  physisorption isotherms and Ar physisorption isotherms on a Micromeritics 3Flex surface analyzer at 77 K after evacuating the samples at 623 K for 12 h under vacuum. From the  $\text{N}_2$  isotherms, the specific surface area ( $S_{\text{BET}}$ ) was determined using the BET method ( $p/p^0$  0.05–0.3). A *t*-plot analysis was used to obtain the specific micropore volume ( $V_{\text{micro}}$ ) and the external surface area ( $S_{\text{ext}}$ ). The total pore volume ( $V_{\text{tot}}$ ) was determined from the amount of  $\text{N}_2$  adsorbed at  $p/p^0$  0.99 and the mesopore volume ( $V_{\text{meso}}$ ) was calculated from the difference between total pore volume and micropore volume. From the Ar isotherms, the median pore width was determined using the Horvath–Kawazoe model. FTIR spectra of self-supporting wafers using pyridine as probe molecule were recorded following a previously published procedure<sup>55</sup> and using the molar extinction coefficients of Emeis<sup>56</sup> to evaluate the number of acid sites.

**Catalytic Experiments. Esterification.** Liquid phase esterification of ethanol with acetic acid was performed in glass crimp cap vials at 70 °C using 15 mg catalyst and an acetic acid/catalyst weight ratio of 2.5. Ethanol was used in excess (molar ratio ethanol/acetic acid 10) and the conversion was calculated based on acetic acid. Samples were analyzed on a Shimadzu 2010 GC equipped with a 60 m DB-FFAP column and a flame ionization detector (FID).

**Alkylation.** Liquid phase alkylation of toluene with benzyl alcohol was performed in glass crimp cap vials at 100 °C using 16 mg of catalyst, 80 mg of benzylalcohol and a molar toluene/benzylalcohol ratio of 100. Prior to reaction, the catalysts were dried overnight at 200 °C and the reaction was performed under  $\text{N}_2$  atmosphere using dried reactants. Samples were analyzed on a Shimadzu 2010 GC equipped with a 60 m CP-Sil-5 column and an FID.

## ■ RESULTS AND DISCUSSION

**Physicochemical Properties of the Interlayer Expanded Materials.** All three different interlayer expansion

**Table 1.** Composition, Structure and Texture of Samples Obtained after Interlayer Expansion of Al-RUB-36

entry	expansion treatment	structure	Si/Al <sup>a</sup>	$S_{\text{BET}}$ ( $\text{m}^2/\text{g}$ )	$S_{\text{ext}}$ ( $\text{m}^2/\text{g}$ )	$V_{\text{tot}}$ ( $\text{cm}^3/\text{g}$ )	$V_{\text{micro}}$ ( $\text{cm}^3/\text{g}$ )	$V_{\text{meso}}$ ( $\text{cm}^3/\text{g}$ )
1	DCDMS, HCl	IEZ-CDO	336	327	58	0.25	0.14	0.11
2	DEDMS, $\text{H}_2\text{SO}_4$	IEZ-CDO	177	359	41	0.30	0.16	0.14
3	$\text{H}_2\text{SO}_4$	IEZ-CDO	174	350	49	0.25	0.16	0.09

<sup>a</sup>ICP.

treatments of Al-RUB-36 result in an expanded material corresponding to Al-COE-4 (IEZ-CDO). The XRD patterns (Figure S1, Supporting Information) are very similar, showing the typical shift of the first and most dominant reflection toward lower angles, compared to the parent Al-RUB-36 material.  $N_2$  physisorption (Table 1, Figure S2, Supporting Information) demonstrates the microporous nature of the materials with low  $N_2$  uptake at higher relative pressures. However, the different interlayer expansion approaches result in differences in Al-content and speciation. Although all expanded samples have a higher bulk Si/Al ratio than the Al-RUB-36 precursor (Si/Al = 102), the Al-COE-4s obtained from chloride-free synthesis clearly have a higher Al-content than Al-COE-4 obtained using DCDMS and HCl (Table 1). The  $^{27}\text{Al}$  MAS NMR spectrum (Figure 1) of the latter only shows a

result in Al removal from the framework, but that in the case using DCDMS and HCl, the formed extra-framework Al is removed more effectively from the zeolite. The differences in Al-content and in origin of the bridging atom are expected to influence the structural and textural modifications of the Al-COE-4 materials upon alkaline treatment, as shown in the next sections.

#### Alkaline Treatments. Alkaline Treatment of Al-COE-4.

The influence of an alkaline treatment on the structure, texture and composition of Al-COE-4 was investigated for the three types of interlayer expanded materials (Tables 2–4). NaOH was initially used as the source of alkalinity; it was gradually replaced by TPAOH. The XRD patterns reveal that treatments using 0.2 M NaOH result in the complete destruction of the framework whereas the use of TPAOH as the sole source of alkalinity preserves the framework topology for all three Al-COE-4 types. Even the addition of a small amount of Al to the 0.2 M NaOH solution, which has been reported to protect Si-rich zeolites from unselective dissolution in alkaline media,<sup>53</sup> does not suffice to maintain the zeolite structure (entry 3 in Tables 2–4). By partially replacing NaOH by TPAOH, the Si/Al ratio of the product decreases and after calcination the FER topology is obtained with an interlayer distance related 200 reflection at  $2\theta = 9.4^\circ$ , indicating that the original ferrierite layer structure was preserved but the layers reconnected in a different fashion to form the FER topology rather than CDO (200 at  $2\theta = 9.6^\circ$ ) or the interlayer expanded CDO (200 at  $2\theta = 7.5^\circ$ ) (Figure 2). This indicates that during these treatments with intermediate TPAOH concentration, at least one of the bonds between the bridging Si atom and the layers has been severed, allowing the disconnected layers to recombine into the FER topology. This selective removal of bridging Si atoms can easily be explained: first, these atoms have only two connections to the rest of the framework, and second, they are easily accessible, as they are located in the interlayer gallery. Both features render these atoms more susceptible to removal via alkaline leaching compared to the T atoms of the original layer. The additional sliding in the stacking order of the disconnected ferrierite type layers toward a FER-type stacking has also been observed by Zhao et al.:<sup>25</sup> swelling of the layered precursor RUB-36 with cetyltrimethylammonium hydroxide followed by deswelling in acid conditions and calcination also resulted in FER rather than CDO topology.  $N_2$  and Ar physisorption (Figures 3 and S3 (Supporting Information) and Tables 2–4) show that this transformation from IEZ-CDO to FER is accompanied by a substantial loss of micropore volume and a decrease in median pore width, but also by a significant increase in mesopore volume and external surface area. The latter increases up to even more than four times the original value.

Use of TPAOH as the sole source of alkalinity preserves the structure, texture and composition of the parent Al-COE-4 materials rather well. The XRD patterns show the same reflections as the parent IEZ-CDO at the same positions (Figure 2c,f). Moreover, the mass yields are high (>89%),

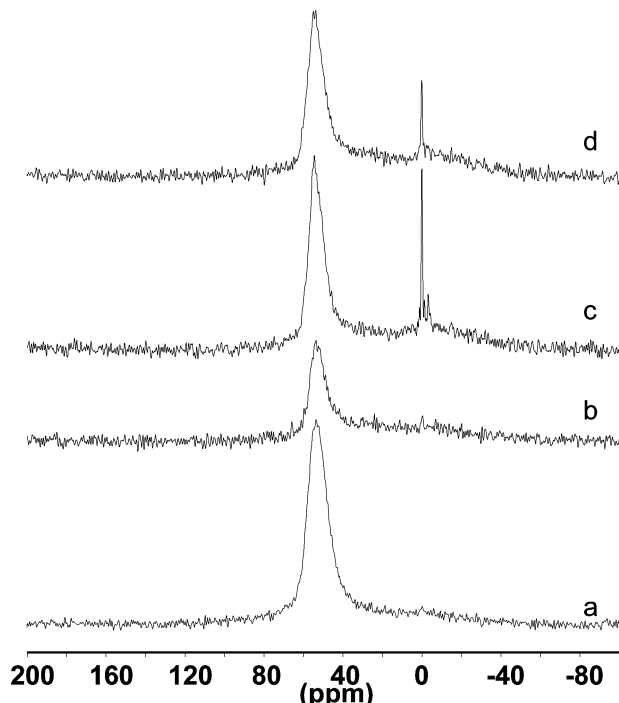


**Figure 1.**  $^{27}\text{Al}$  MAS NMR spectra of Al-RUB-37 (a) and of Al-COE-4 obtained via interlayer expansion using DCDMS and HCl (b), DEDMS and  $\text{H}_2\text{SO}_4$  (c) and  $\text{H}_2\text{SO}_4$  (d).

signal at 54 ppm corresponding to tetrahedrally coordinated framework species, whereas the other two materials show an additional broad signal around 0 ppm superimposed on a narrow signal. These signals are typically assigned to octahedrally coordinated extra-framework Al-species.<sup>57</sup> The spectrum of Al-RUB-37 derived from the same Al-RUB-36 precursor on the other hand, only shows a signal at 54 ppm, too, but with a higher signal intensity than Al-COE-4 from DCDMS and HCl treatment. The differences in Al content and speciation imply that all three interlayer expansion methods

**Table 2. Yield, Composition, Structure and Texture of Samples Obtained after Alkaline Treatment of Al-COE-4 (DCDMS, HCl)**

entry	treatment <sup>a</sup>	yield (%)	structure	Si/Al <sup>b</sup>	$S_{\text{BET}}$ ( $\text{m}^2/\text{g}$ )	$S_{\text{ext}}$ ( $\text{m}^2/\text{g}$ )	$V_{\text{tot}}$ ( $\text{cm}^3/\text{g}$ )	$V_{\text{micro}}$ ( $\text{cm}^3/\text{g}$ )	$V_{\text{meso}}$ ( $\text{cm}^3/\text{g}$ )
1			IEZ-CDO	336	327	58	0.25	0.14	0.11
2	0.2 M NaOH		amorphous						
3	0.2 M NaOH, 0.003 M $\text{Al(OH)}_4^-$		amorphous						
4	0.025 M TPAOH	51	FER	177	176	114	0.28	0.03	0.25
5	0.1 M TPAOH	39	FER	272	84	68	0.20	0.01	0.19
6	0.2 M TPAOH	95	IEZ-CDO	308	326	40	0.26	0.15	0.11
7	0.1 M DEDMAOH	85	collapsed	302	22	16	0.06	<0.01	0.05
8	0.2 M DEDMAOH	94	IEZ-CDO	265	328	28	0.25	0.16	0.09

<sup>a</sup>In entries 2–8, for base concentrations between 0.2 M, NaOH was added to bring the  $[\text{OH}^-]$  at 0.2 M. <sup>b</sup>ICP.

**Table 3. Yield, Composition, Structure and Texture of Samples Obtained after Alkaline Treatment of Al-COE-4 (DEDMS,  $\text{H}_2\text{SO}_4$ )**

entry	treatment <sup>a</sup>	yield (%)	structure	Si/Al <sup>b</sup>	$S_{\text{BET}}$ ( $\text{m}^2/\text{g}$ )	$S_{\text{ext}}$ ( $\text{m}^2/\text{g}$ )	$V_{\text{tot}}$ ( $\text{cm}^3/\text{g}$ )	$V_{\text{micro}}$ ( $\text{cm}^3/\text{g}$ )	$V_{\text{meso}}$ ( $\text{cm}^3/\text{g}$ )
1			IEZ-CDO	177	359	41	0.30	0.16	0.14
2	0.2 M NaOH		amorphous						
3	0.2 M NaOH, 0.003 M $\text{Al(OH)}_4^-$		amorphous						
4	0.025 M TPAOH	51	FER	106	380	187	0.42	0.10	0.32
5	0.1 M TPAOH	62	FER	128	346	152	0.39	0.10	0.29
6	0.2 M TPAOH	89	IEZ-CDO	215	360	25	0.23	0.17	0.06
7	0.1 M DEDMAOH	80	collapsed	177	38	15	0.08	0.01	0.07
8	0.2 M DEDMAOH	96	IEZ-CDO	183	348	29	0.26	0.16	0.10

<sup>a</sup>In entries 2–8, for base concentrations between 0.2 M, NaOH was added to bring the  $[\text{OH}^-]$  at 0.2 M. <sup>b</sup>ICP.

**Table 4. Yield, Composition, Structure and Texture of Samples Obtained after Alkaline Treatment of Al-COE-4 ( $\text{H}_2\text{SO}_4$  only)**

entry	treatment <sup>a</sup>	yield (%)	structure	Si/Al <sup>b</sup>	$S_{\text{BET}}$ ( $\text{m}^2/\text{g}$ )	$S_{\text{ext}}$ ( $\text{m}^2/\text{g}$ )	$V_{\text{tot}}$ ( $\text{cm}^3/\text{g}$ )	$V_{\text{micro}}$ ( $\text{cm}^3/\text{g}$ )	$V_{\text{meso}}$ ( $\text{cm}^3/\text{g}$ )
1			IEZ-CDO	174	350	49	0.25	0.16	0.09
2	0.2 M NaOH		amorphous						
3	0.2 M NaOH, 0.003 M $\text{Al(OH)}_4^-$		amorphous						
4	0.025 M TPAOH	57	FER	102	243	136	0.29	0.06	0.23
5	0.1 M TPAOH		amorphous						
6	0.2 M TPAOH	85	IEZ-CDO	218	263	30	0.19	0.12	0.07
7	0.1 M DEDMAOH	83	collapsed	207	59	32	0.12	0.01	0.11
8	0.2 M DEDMAOH	91	IEZ-CDO	153	164	31	0.15	0.07	0.08

<sup>a</sup>In entries 2–8, for base concentrations between 0.2 M, NaOH was added to bring the  $[\text{OH}^-]$  at 0.2 M. <sup>b</sup>ICP.

indicating very little dissolution. Clearly, the amount of  $\text{TPA}^+$  present here suffices to preserve even the Si-rich structure of Al-COE-4 obtained using DCDMS and HCl. For both Al-COE-4 materials obtained using silylating agents (Tables 2 and 3), even a small increase in micropore volume and a decrease in external surface area can be observed. This may be explained by the removal of a minor amount of debris formed in the interlayer expansion treatment, whereas the zeolite crystals remain protected by the  $\text{TPA}^+$  resulting in higher micropore volumes per mass, and lower (intercrystalline) mesopore volumes and external surface areas. The origin of the debris could be, for instance, unselective condensation of silylating agents or some degradation of the layers during the interlayer expansion treatment. This degradation is known to occur to a certain extent, as this is the source for bridging Si atoms when no silylating agent is used. SEM images support the hypothesis of debris removal: the materials demonstrate a more homogeneous plate-like morphology with even more clean and smooth surfaces after treatment with 0.2 M TPAOH than their parent Al-COE-4 materials (Figures 4, S4 and S5, Supporting Information). On the other hand, in the case of Al-COE-4 from  $\text{H}_2\text{SO}_4$  only, alkaline treatment with 0.2 M

TPAOH results in a clear decrease in micropore volume without the formation of additional mesoporosity (Table 4). This can be attributed to a lower stability of the framework and subsequent partial collapse due to an insufficient number of bridging Si atoms.<sup>58</sup>

As indicated above, the influence of the different treatments is also reflected in morphological changes (Figures 4, S4 and S5, Supporting Information). Treatment of Al-COE-4 from DEDMS and  $\text{H}_2\text{SO}_4$  with 0.1 M NaOH and 0.1 M TPAOH results not only in a topology transformation of IEZ-CDO to FER (vide supra), but also in severe surface roughening and dissolution from the crystal plate edges (Figure 4c). However, the original plate-like morphology can still be recognized. Using only 0.2 M TPAOH as the source of alkalinity, the surface remains smooth, as mentioned earlier, but with a small amount of macropore formation perpendicular to the crystal plates, consistent with the high yields and preserved textural features. For Al-COE-4 from DCDMS and HCl synthesis, similar observations can be made (Figure S4, Supporting Information). In the case of Al-COE-4 from  $\text{H}_2\text{SO}_4$  only (Figure S5, Supporting Information), the surface roughening at intermediate TPAOH concentration is less pronounced, but the

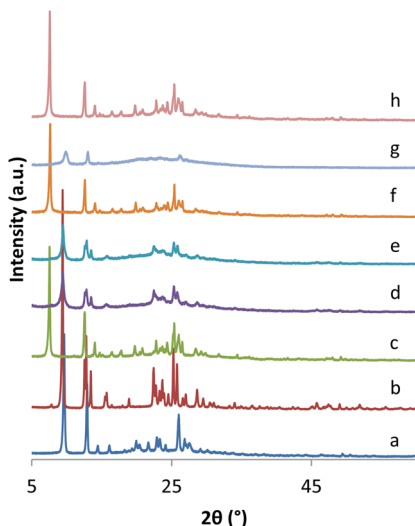


**Figure 2.** XRD patterns of Al-RUB-37 (a), FER (b, obtained from the topotactic condensation of its layered precursor PREFER, according to ref 6), and Al-COE-4 from DEDMS and  $\text{H}_2\text{SO}_4$  synthesis: as-synthesized (c), after alkaline treatment with 0.025 M TPAOH (d), 0.1 M TPAOH (e), 0.2 M TPAOH (f), 0.1 M DEDMAOH (g) and 0.2 M DEDMAOH (h).

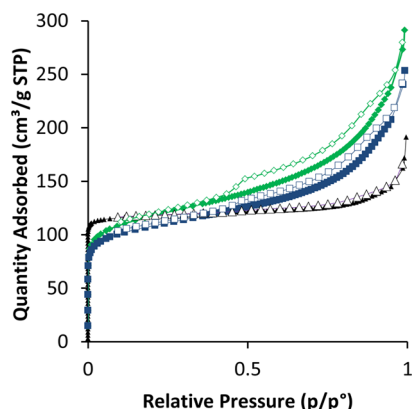


**Figure 3.** Nitrogen physisorption isotherms of Al-COE-4 from DEDMS and  $\text{H}_2\text{SO}_4$  synthesis treated with 0.025 M TPAOH ( $\blacklozenge/\lozenge$ , FER topology), or with 0.1 M TPAOH ( $\blacksquare/\square$ , FER topology) clearly show a higher  $\text{N}_2$  uptake at intermediate relative pressures than the untreated Al-COE-4 material ( $\blacktriangle/\Delta$ , IEZ-CDO). Filled symbols = adsorption; open symbols = desorption.

dissolution from the crystal edges in the case of 0.2 M TPAOH can easily be seen.

The observations of increased preservation of structural, textural and morphological properties upon gradual replacement of NaOH with TPAOH are in agreement with previous reports on the protective effect of the  $\text{TPA}^+$  cation on zeolite surfaces.<sup>53</sup> However, interlayer expanded zeolites differ from the typically investigated zeolite topologies in that they contain bridging Si atoms and hence are not composed of a fully tetrahedrally connected framework. On the one hand, using 0.2 M TPAOH and no NaOH still results in limited framework dissolution and mesopore formation. On the other hand, lowering the  $\text{TPA}^+$  concentration to allow for mesopore formation also results in the selective removal of the weak spots of the framework, i.e., the bridging Si atoms. This results in the remarkable feature that in one step, not only the texture of the zeolite is changed but also its structure. This selective removal

of specific framework elements resulting in the transformation of a 3D zeolite (Al-COE-4) into a different yet related framework with the same type of layers (FER) bears resemblance to the various transformations of the 3D UTL framework into, for instance, OKO or PCR topologies.<sup>14,19</sup>

In an attempt to investigate whether the bridging Si atom could be removed without shifting toward FER-type stacking, the original OSDA of the layered precursor RUB-36, DEDMAOH, was used as a source of alkalinity instead of TPAOH. From the XRD pattern (Figure 2h), it is clear that using 0.2 M DEDMAOH, as with 0.2 M TPAOH, the IEZ-CDO structure is preserved. However, partial replacement of DEDMAOH by NaOH again results in a modification of the structure with a drastic reduction of the micropore volume (entry 7 in Tables 2–4 and Figure S3, Supporting Information). Besides the halo typical for amorphous silica between 20 and  $30^\circ 2\theta$ , some weak, broad reflections can still be observed in the XRD pattern (Figure 2g). The pattern does not seem to correspond to any of the known RUB-36 related materials and it would seem that the presence of DEDMA<sup>+</sup> did not result in the preservation of the bridging Si or the organization of the layers into the CDO type stacking. Given the low *d*-value of the first and most intense reflection at  $2\theta = 9.9^\circ$  (8.96 Å), it is possible that the bridging Si atom was again removed and the layers condensed into a rather disordered type of stacking, even more closely spaced than in CDO. A similar type of disordered condensation of layers can be found in the case of NU-6(1), which is a layered precursor of the NSI topology. In this case, calcination after OSDA removal through acid treatment no longer results in congruent condensation of the interlayer surface silanols into the NSI topology. According to Roth and Kresge,<sup>59</sup> the removal of the template most likely causes a mismatch between the silanol groups on the opposite sides of the interlayer gallery which results in a disordered, collapsed and contracted structure upon calcination with a *d*-spacing even lower than that of the ordered topotactic condensation product of NU-6(1). The low *d*-space value observed in the XRD-pattern of Figure 2g and the low quality of the pattern would suggest a similarly collapsed and contracted structure. The product of this type of noncongruent, disordered stacking of layers has been referred to as a “subzeolite” and has not only been found for the NSI-topology but also for the FER topology starting from the lamellar precursor PLS-3.<sup>32,59,60</sup>

**Alkaline Treatment of Al-COE-3.** In a next step, we investigated the modifications upon alkaline treatment of the interlayer expanded zeolites before calcination, i.e., Al-COE-3 type materials (Tables 5 and 6). In this case, the presence of methyl groups from the silylating agent increases the hydrophobicity of the materials,<sup>54</sup> and this is expected to influence the stability in the alkaline treatment. Tables 5 and 6 show that the structure of the parent material is preserved under all investigated conditions. Even the more severe treatment that uses NaOH as the sole source of alkalinity does not result in a topology modification. For Al-COE-3 obtained from DCDMS and HCl synthesis, this higher stability of the layer and of the incorporated bridging Si atoms is to be ascribed to the methyl groups attached to the bridging Si atoms. In Al-COE-3 obtained using only  $\text{H}_2\text{SO}_4$ , there are no methyl groups on the bridging Si atoms. The increased stability should therefore be attributed to the presence of residual OSDA,<sup>38</sup> which is not always fully removed during the interlayer expansion treatment,<sup>61</sup> and which seems to increase

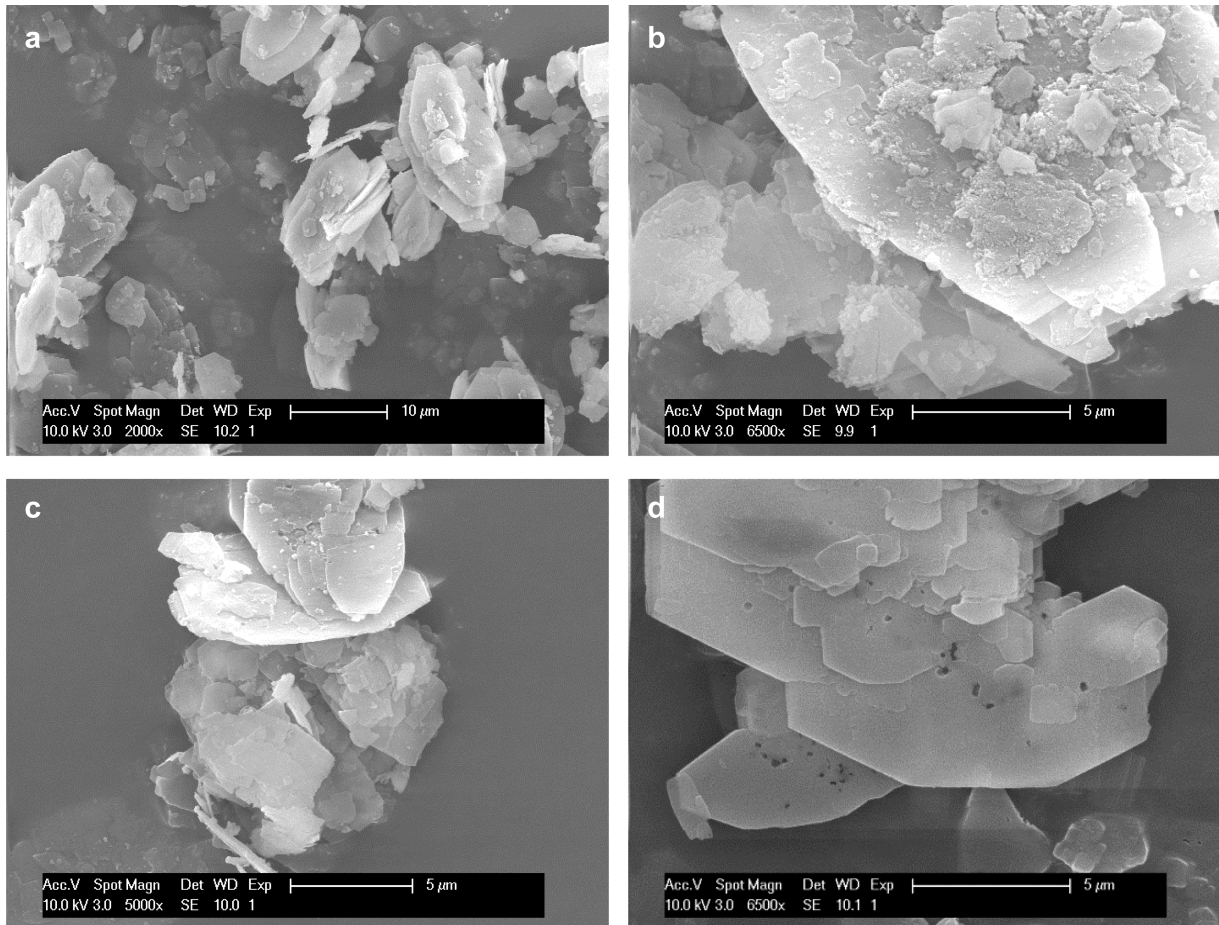


**Figure 4.** SEM images of Al-COE-4 from DEDMS and H<sub>2</sub>SO<sub>4</sub> synthesis: as synthesized (a), after treatment with 0.025 M TPAOH, resulting in FER (b), after treatment with 0.1 M TPAOH, resulting in FER (c) and after treatment with 0.2 M TPAOH (d).

**Table 5. Yield, Composition, Structure and Texture of Samples Obtained after Alkaline Treatment of Al-COE-3 (DCDMS, HCl)**

entry	treatment <sup>a</sup>	yield (%)	structure	Si/Al <sup>b</sup>	S <sub>BET</sub> (m <sup>2</sup> /g)	S <sub>ext</sub> (m <sup>2</sup> /g)	V <sub>tot</sub> (cm <sup>3</sup> /g)	V <sub>micro</sub> (cm <sup>3</sup> /g)	V <sub>meso</sub> (cm <sup>3</sup> /g)
1			IEZ-CDO	336	327	58	0.25	0.14	0.11
2	0.2 M NaOH	64	IEZ-CDO	252	256	45	0.25	0.11	0.14
3	0.2 M NaOH, 0.003 M Al(OH) <sub>4</sub> <sup>-</sup>	67	IEZ-CDO	87	262	63	0.24	0.10	0.14
4	0.025 M TPAOH	63	IEZ-CDO	275	294	59	0.27	0.12	0.15
5	0.1 M TPAOH	81	IEZ-CDO	288	290	53	0.25	0.12	0.13
6	0.2 M TPAOH	89	IEZ-CDO	304	356	29	0.25	0.17	0.08
7	0.2 M DEDMAOH	90	IEZ-CDO	257	337	20	0.24	0.16	0.08

<sup>a</sup>In entries 2–8, for base concentrations between 0.2 M, NaOH was added to bring the [OH<sup>-</sup>] at 0.2 M. <sup>b</sup>ICP.

**Table 6. Yield, Composition, Structure and Texture of Samples Obtained after Alkaline Treatment of Al-COE-3 (H<sub>2</sub>SO<sub>4</sub> only)**

entry	treatment <sup>a</sup>	yield (%)	structure	Si/Al <sup>b</sup>	S <sub>BET</sub> (m <sup>2</sup> /g)	S <sub>ext</sub> (m <sup>2</sup> /g)	V <sub>tot</sub> (cm <sup>3</sup> /g)	V <sub>micro</sub> (cm <sup>3</sup> /g)	V <sub>meso</sub> (cm <sup>3</sup> /g)
1			IEZ-CDO	174	350	49	0.25	0.16	0.09
2	0.2 M NaOH	69	IEZ-CDO	159	372	77	0.35	0.15	0.20
3	0.2 M NaOH, 0.003 M Al(OH) <sub>4</sub> <sup>-</sup>	62	IEZ-CDO	59	342	81	0.33	0.13	0.20
4	0.025 M TPAOH	65	IEZ-CDO	115	327	60	0.31	0.13	0.18
5	0.1 M TPAOH	81	IEZ-CDO	185	330	64	0.31	0.14	0.17
6	0.2 M TPAOH	92	IEZ-CDO	224	361	27	0.24	0.17	0.07

<sup>a</sup>In entries 2–8, for base concentrations between 0.2 M, NaOH was added to bring the [OH<sup>-</sup>] at 0.2 M. <sup>b</sup>ICP.

the hydrophobicity of the material, and hence its resilience to aqueous base. The same effect could add to the stability of Al-COE-3 obtained from DCDMS and HCl synthesis. To verify whether residual OSDA could be present in the Al-COE-3 type

parent materials, thermogravimetric analyses were performed. These showed a weight loss between 200 and 550 °C of 1.4 wt % for the DCDMS and HCl expansion (which includes the two geminal methyl groups), and 1.6 wt % using only H<sub>2</sub>SO<sub>4</sub>

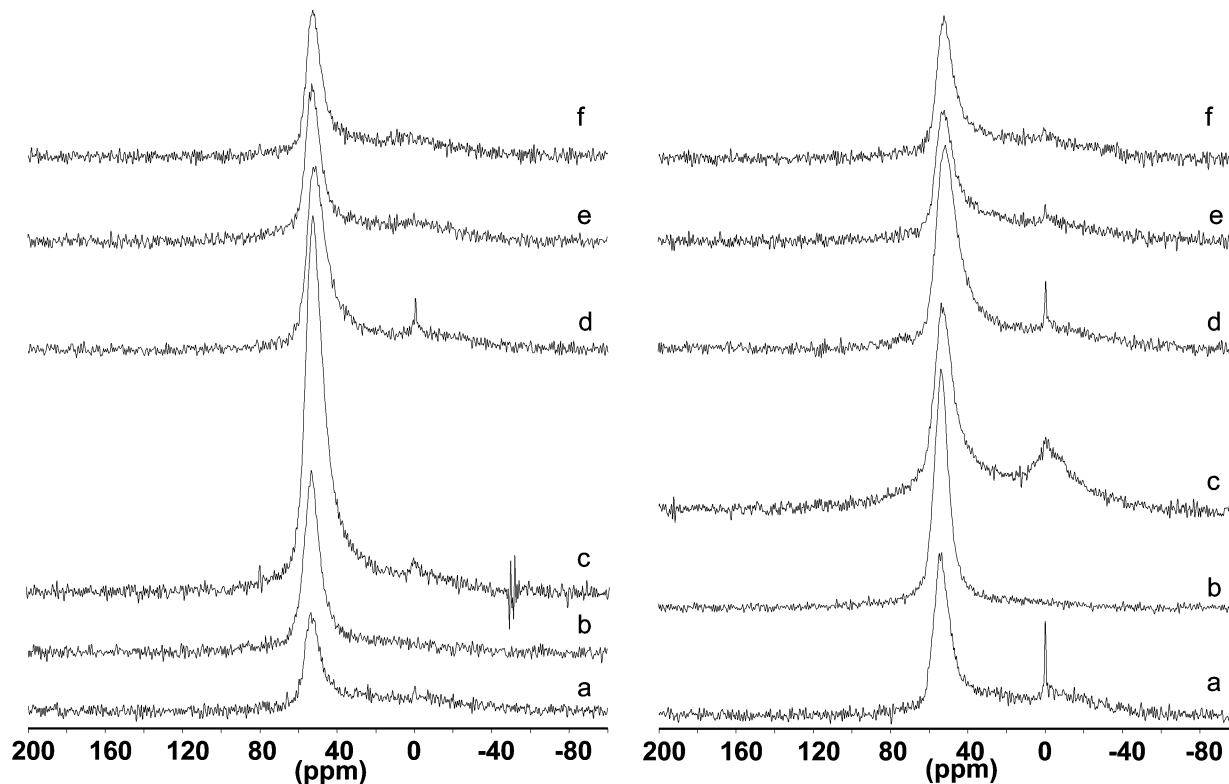


**Figure 5.**  $^{27}\text{Al}$  MAS NMR spectra of the Al-COE-3 type materials as synthesized (a), after treatment with 0.2 M NaOH (b), with 0.2 M NaOH and 0.003 M  $\text{Al(OH)}_4^-$  (c), with 0.2 M NaOH and 0.003 M  $\text{Al(OH)}_4^-$  followed by acid treatment (d), with 0.025 M TPAOH (e) and with 0.1 M TPAOH (f). The spectra on the left are for Al-COE-3 from DCDMS and HCl synthesis, spectra on the right are for Al-COE-3 from  $\text{H}_2\text{SO}_4$ -only synthesis. Spectra were collected on calcined and ion-exchanged materials.

(Figure S6, Supporting Information). These values are much lower than the 14.5 wt % observed for RUB-36 but could still explain the higher stability of these Al-COE-3 type materials. Moreover, as an indication of the hydrophilicity of the samples, the weight loss between room temperature and 200 °C was also determined for samples pre-equilibrated with a controlled humidity. In the case of Al-COE-3 obtained from  $\text{H}_2\text{SO}_4$ -only synthesis, a value of 1.2 wt % was found whereas for the corresponding Al-COE-4 material, this increased up to 5.0 wt %, indicating that the calcined Al-COE-4 is hydrophilic and the noncalcined Al-COE-3 is much more hydrophobic, even if no silylating agent was used in the interlayer expansion leading to Al-COE-3. The increased stability of Al-COE-3 against alkaline leaching is also evident from the SEM images of the samples (Figures S7 and S8, Supporting Information). They maintain a smooth surface without the roughening so frequently observed after alkaline treatment of the calcined Al-COE-4 type materials. In addition, the formation of macropores perpendicular to the crystal plates is often observed, especially in the presence of NaOH but much less when only TPAOH is used as alkaline source.

The textural properties of the alkaline treated Al-COE-3 type materials are shown in Tables 5 and 6. Using only NaOH, an increase in mesopore volume is observed accompanied by a reduction of the micropore volume. The effect is much more pronounced for the  $\text{H}_2\text{SO}_4$ -only type expansion, which would again indicate a somewhat lower stability, even for the uncalcined form. The textural modifications are much less pronounced for the DCDMS and HCl expansion. A small amount of Al was added to evaluate its pore-directing effect for the Si-rich Al-COE-3 obtained from DCDMS and HCl

treatment. Although the impact on the yield and texture is rather limited, it is clear from the decreased Si/Al ratio that this additional Al was not washed away and remained in the sample. Moreover, the  $^{27}\text{Al}$  MAS NMR spectrum (Figure 5c) clearly shows a strong enhancement of the 54 ppm signal in addition to the appearance of a broad signal around 0 ppm, which is not observed when using only NaOH in the alkaline treatment. The latter signal shows that some of the additional Al ends up as extra-framework Al, whereas the increase of the former signal would indicate (partial) incorporation of the externally added Al into the zeolite. After a mild acid treatment, however, the 54 ppm signal intensity (Figure 5d) is again strongly reduced, meaning that the extra integrated Al is rather easily removed from the zeolite. These findings are in agreement with previous studies reporting Al incorporation in silicalite-1 treated under similar conditions.<sup>53</sup> From the  $^{27}\text{Al}$  MAS NMR spectra, it is also clear that the alkaline treatments in the presence of TPAOH resulted in the appearance of a weak, broad band around 0 ppm indicating the transformation of part of the Al to extra-framework species. Analogous observations can be made for the  $^{27}\text{Al}$  MAS NMR spectra of the alkaline treated Al-COE-3 from the  $\text{H}_2\text{SO}_4$ -only type expansion (Figure 5).

Like for the alkaline treatments of the calcined materials, the mesopore volume decreased with increasing replacement of NaOH by TPAOH, whereas the micropore volume, yield and Si/Al ratios increased. However, for the uncalcined Al-COE-3 type materials, the changes are less drastic, especially regarding textural properties, which can be ascribed to the higher stability because of the methyl groups and residual OSDA. The highest external surface areas are obtained using only NaOH as source of alkalinity and with the addition of 0.003 M  $\text{Al(OH)}_4^-$ , the

**Table 7.** Acid Properties and Conversions in the Esterification of Acetic Acid with Ethanol and in the Alkylation of Toluene with Benzyl Alcohol, Both after 2 h of Reaction<sup>a</sup>

entry	interlayer expansion	alkaline treatment <sup>b</sup>	BAS ( $\mu\text{mol/g}$ ) <sup>c</sup>	LAS ( $\mu\text{mol/g}$ ) <sup>c</sup>	conversion (%)	
					acetic acid	benzyl alcohol
1	no catalyst				2.6	<0.1
2	DCDMS, HCl		1.4	7.4	9.1	4.5
3	DCDMS, HCl	0.2 M NaOH	1.9	5.8	6.7	0.85
4	DCDMS, HCl	0.2 M NaOH, 0.003 M $\text{Al(OH)}_4^-$	2.6	6.3	7.1	9.7
5	DCDMS, HCl	0.025 M TPAOH	2.3	4.6	5.6	2.6
6	$\text{H}_2\text{SO}_4$		2.9	4.0	9.9	27
7	$\text{H}_2\text{SO}_4$	0.2 M NaOH	8.5	4.1	6.2	4.1
8	$\text{H}_2\text{SO}_4$	0.2 M NaOH, 0.003 M $\text{Al(OH)}_4^-$	13	14	7.2	26
9	$\text{H}_2\text{SO}_4$	0.025 M TPAOH	3.3	5.2	7.4	6.2

<sup>a</sup>Results are given for the Al-COE-4 type materials from different interlayer expansion treatments and for selected alkaline treatments of their Al-COE-3 type counterparts. <sup>b</sup>Alkaline treatment was performed at the Al-COE-3 stage. Acid and catalytic properties were evaluated after calcination and ion exchange, i.e., at the Al-COE-4 stage. <sup>c</sup>Amount of pyridine adsorbed on Bronsted acid sites (BAS) and Lewis acid sites (LAS) as determined from the respective IR absorption bands at 150 °C.

effect being more significant on Al-COE-3 from  $\text{H}_2\text{SO}_4$ -only synthesis. As was also observed for the calcined materials, using only TPAOH actually increases the micropore volume to values higher than those of the untreated counterparts and lower mesopore volumes. This can again be attributed to the removal of debris without significant modification of the crystalline part.

**Alkaline Treatment of RUB-36.** The possibility of obtaining mesoporous Al-COE-4 by subjecting the layered precursor Al-RUB-36 first to an alkaline treatment followed by interlayer expansion was also investigated. The influence of framework Al was investigated by subjecting purely siliceous RUB-36 to the same treatments. For simplicity, the layered precursors were first only alkaline treated and calcined directly without intermediate interlayer expansion. Therefore, the structural and textural characteristics should be compared with those of the merely calcined RUB-36, i.e., its topotactic condensation product RUB-37 with CDO topology.

After all applied alkaline treatments, direct calcination resulted in the CDO topology; no transformation toward FER or any other topology was observed (Tables S1 and S2, Supporting Information). This is due to the large amount of OSDA initially present in between the layers, which stays there throughout the alkaline treatment. Logically, the IEZ-CDO topology was obtained in those cases where an expansion treatment was applied. All treatments using the standard conditions of 0.2 M  $\text{OH}^-$  for 0.5 h at 65 °C resulted in high yields (>80%) and only minor changes in textural properties. The morphology is also preserved without any surface roughening but a small number of macropores perpendicular to the crystal plates could be observed (Figures S9 and S10, Supporting Information). The lack of extensive modifications under these standard conditions once more demonstrates the protective effect of the intercalated OSDA on the (alumino)-silicate layers. For both Al-RUB-36 and purely siliceous RUB-36, the highest mesopore volumes and external surface areas were obtained using only NaOH. To increase this effect, harsher treatments using longer reaction times and/or higher temperatures and NaOH concentrations were used on Al-RUB-36. This resulted indeed in a higher removal of material as can be seen from the lower yields, and using 0.4 M NaOH at 75 °C for 2 h, the mesopore volume even more than doubled. However, the fact that the external surface area hardly increased (57 m<sup>2</sup>/g compared to 55 m<sup>2</sup>/g without alkaline treatment) indicates that most of the dissolution occurred unselectively at

the crystal edges. This is also evident from the SEM images (Figure S9, Supporting Information), which additionally show the formation of large macropores through the crystal plates.

The effect of additional Al on the textural modifications of purely siliceous RUB-36 was also investigated (Table S2, entries 3 and 4, Supporting Information). As can be seen from the Si/Al ratios and the <sup>27</sup>Al MAS NMR spectra (Figure S11, Supporting Information), the added Al remains in the zeolite after alkaline treatment, but is mostly removed after interlayer expansion. Remarkably, the interlayer expansion treatment doubled the external surface area. In an attempt to increase the amount of residual Al after interlayer expansion and to study the effect on the textural properties, the amount of added Al was increased by a factor 10 (Table S2, entries 5 and 6, Supporting Information). Elemental analysis showed indeed an increase in the Al incorporation after alkaline treatment, and the <sup>27</sup>Al MAS NMR spectrum showed correspondingly higher signal strengths. However, the subsequent interlayer expansion did not show the expected increase in mesoporosity, which again demonstrates the importance of the optimal concentration of pore-directing agents during alkaline treatments. Why the increase in external surface area only shows up in the case of the purely siliceous RUB-36 and only after interlayer expansion is, however, unclear. One explanation could be that on the one hand, using 0.03 M  $\text{Al(OH)}_4^-$ , the zeolite surface is too well protected to extract Si. On the other hand, using 0.003 M  $\text{Al(OH)}_4^-$ , the framework is partially destroyed but the debris is only removed during the acidic interlayer expansion treatment, opening up the formed mesopores. The removal of this newly incorporated Al upon interlayer expansion implies the loss of potential catalytically active sites. However, alternative interlayer expansion methods using more complex silylating agents or incorporating different heteroatoms have been proposed before to introduce catalytic activity.<sup>55,61</sup> Combining this alkaline treatment with those interlayer expansion methods could offer new ways for obtaining hierarchical catalysts from RUB-36. The total mesopore volume and external surface area obtained in this modification may still be rather low in comparison to other topologies, but this is likely related to the crystal morphology. Verboekend and Pérez-Ramírez noted that plate-like and needle-like crystal morphologies generally result in lower desilication efficiencies and external surfaces.<sup>62</sup> They also pointed out that as in these type of crystals, the channels frequently run along the longer crystal

dimension, introduction of a small number of mesopores along the shortest crystal dimension, perpendicular to the micropores, could still result in a significant increase of the accessibility of the micropores in the center of the crystal.

**Catalytic Experiments.** The acid properties and the conversion of acetic acid in the esterification with ethanol and of benzyl alcohol in the alkylation of toluene are shown in Table 7 for selected samples. In the alkaline treatment of the Al-COE-4 type of materials, the introduction of mesoporosity was always accompanied by a transformation to a different topology. Therefore, only catalytic results of catalysts that had been alkaline treated at the Al-COE-3 stage are shown. Characterization of the acidity using Fourier transform infrared spectroscopy (FTIR) with pyridine as the probe molecule shows that after alkaline treatment, both Brønsted and Lewis acid sites remain present in the catalysts. In the alkylation of toluene, alkaline treatment in the presence of additionally added Al proved to be successful in preserving and even improving the activity (Table 7, entries 4 and 8). On the other hand, the alkaline treatments negatively impacted the catalytic activity of the materials in the esterification reactions, despite the higher Al content. The lower activity could be caused by a number of factors. First, there is a loss of BET surface area and micropore volume after alkaline treatment in the case of Al-COE-4 from DCDMS and HCl expansion (Table 5). Second, a change in the Al speciation and accessibility could also result in significant changes in acid properties, even though these are not easily observed from the  $^{27}\text{Al}$  MAS NMR spectra. Even though the FTIR characterizations shows an increase in the number of Brønsted acid sites, the acid site strength may also be influenced by the alkaline treatment. In some cases, the alkaline treatment of H-ZSM-5, H-SSZ-13, and  $\beta$ -zeolite also resulted in negative effects on the acidic properties in spite of the higher Al content compared to the nontreated parent materials.<sup>44,63,64</sup>

## ■ CONCLUSION

RUB-36 based materials can be subjected to alkaline treatments in order to create mesoporosity at different stages of their synthesis. The composition of the alkaline solution and the framework hydrophobicity are important factors influencing whether mesopores are created, or whether only macropores are formed in addition to dissolution of the framework from the edges onward. Subjecting RUB-36 itself to alkaline conditions using standard treatment parameters of 0.2 M  $\text{OH}^-$  for 30 min at 65 °C results in only minor changes of the textural properties because the high OSDA content protects the layers. After interlayer expansion, but before calcination, i.e., at the COE-3 stage, the structure of the material is preserved under different treatment conditions and moderate increases in external surface area with minor losses in micropore volume can be obtained. Harsher treatments with a greater proportion of the alkalinity originating from NaOH result in more obvious additional macropore formation. For these materials, the addition of extra Al to the alkaline treatment solution was beneficial for the catalytic activity in alkylation reactions. Calcination of the interlayer expanded RUB-36 materials to COE-4 not only removes any residual OSDA or methyl groups but also increases the hydrophilicity and it also lowered the stability of the materials under alkaline conditions so that both the texture and structure could be modified. The milder treatments using only TPAOH as source of alkalinity generated very few textural and no structural changes; increasing the proportion of NaOH results in a severe surface roughening, the formation of

both meso- and macropores but also structural modifications and an increased loss of material due to unselective dissolution from the edges on. Using the proper combination of TPAOH and NaOH, the materials could be transformed into a highly mesoporous FER-type zeolite. These results add a new case to the large family of possible textural and structural modifications of materials based on layered zeolite precursors.

## ■ ASSOCIATED CONTENT

### § Supporting Information

Additional characterization data (XRD patterns, SEM images,  $\text{N}_2$  and Ar sorption physisorption isotherms, TGA curves, NMR spectra) and tables containing the elemental composition, structure and textural parameters of alkaline treated RUB-36 samples. This material is available free of charge via the Internet at <http://pubs.acs.org>.

## ■ AUTHOR INFORMATION

### Corresponding Author

\*D. E. De Vos. E-mail: dirk.devos@biw.kuleuven.be.

### Notes

The authors declare no competing financial interest.

## ■ ACKNOWLEDGMENTS

T.D.B. acknowledges F.W.O. - Vlaanderen (Research Foundation Flanders) for a Ph.D. fellowship. Support from BASF SE under the INCOE framework is acknowledged.

## ■ REFERENCES

- (1) Maesen, T.; Marcus, B. *Stud. Surf. Sci. Catal.* **2001**, *137*, 1.
- (2) Martens, J. M.; Tielen, M.; Jacobs, P. A.; Weitkamp, J. *Zeolites* **1984**, *4*, 98.
- (3) Tijsebaert, B.; Yilmaz, B.; Müller, U.; Gies, H.; Zhang, W.; Bao, X.; Xiao, F. S.; Tatsumi, T.; De Vos, D. *J. Catal.* **2011**, *278*, 246.
- (4) Blake, A. J.; Franklin, K. R.; Lowe, B. M. *J. Chem. Soc., Dalton Trans.* **1988**, *10*, 2513.
- (5) Ikeda, T.; Akiyama, Y.; Oumi, Y.; Kawai, A.; Mizukami, F. *Angew. Chem.* **2004**, *116*, 5000.
- (6) Schreyeck, L.; Caullet, P.; Mougenel, J. C.; Guth, J. L.; Marler, B. *Microporous Mater.* **1996**, *6*, 259.
- (7) Leonowicz, M. E.; Lawton, J. A.; Lawton, S. L.; Rubin, M. K. *Science* **1994**, *264*, 1910.
- (8) Zanardi, S.; Alberti, A.; Cruciani, G.; Corma, A.; Fornes, V.; Brunelli, M. *Angew. Chem., Int. Ed.* **2004**, *43*, 4933.
- (9) Wang, Y.; Gies, H.; Marler, B.; Müller, U. *Chem. Mater.* **2005**, *17*, 43.
- (10) Marler, B.; Ströter, N.; Gies, H. *Microporous Mesoporous Mater.* **2005**, *83*, 201.
- (11) Moteki, T.; Chaikittisilp, W.; Shimojima, A.; Okubo, T. *J. Am. Chem. Soc.* **2008**, *130*, 15780.
- (12) Rojas, A.; Cambor, M. A. *Chem. Mater.* **2013**, *26*, 1161.
- (13) Asakura, Y.; Takayama, R.; Shibue, T.; Kuroda, K. *Chem.—Eur. J.* **2014**, *20*, 1893.
- (14) Roth, W. J.; Nachtigall, P.; Morris, R. E.; Wheatley, P. S.; Seymour, V. R.; Ashbrook, S. E.; Chlubná, P.; Grajcar, L.; Položíj, M.; Zukal, A.; Shvets, O.; Čejka, J. *Nat. Chem.* **2013**, *5*, 628.
- (15) Asakura, Y.; Osada, S.; Hosaka, N.; Terasawa, T.; Kuroda, K. *Dalton Trans.* **2014**, *43*, 10392.
- (16) Jackowski, A.; Zones, S. I.; Chaudhuri, K.; Lacheen, H. S.; Yeh, S. W. *Microporous Mesoporous Mater.* **2014**, *197*, 33.
- (17) Roth, W. J.; Shvets, O. V.; Shamzhy, M.; Chlubná, P.; Kubů, M.; Nachtigall, P.; Čejka, J. *J. Am. Chem. Soc.* **2011**, *133*, 6130.
- (18) Chlubná-Eliášová, P.; Tian, Y.; Pinar, A. B.; Kubů, M.; Čejka, J.; Morris, R. E. *Angew. Chem.* **2014**, *126*, 7168.
- (19) Verheyen, E.; Joos, L.; Van Haverbekegh, K.; Breynaert, E.; Kasian, N.; Gobechiya, E.; Houthooft, K.; Martineau, C.; Hinterstein,

- M.; Taulelle, F.; Van Speybroeck, V.; Waroquier, M.; Bals, S.; Van Tendeloo, G.; Kirschhock, C. E. A.; Martens, J. A. *Nat. Mater.* **2012**, *11*, 1059.
- (20) Wheatley, P. S.; Chlubná-Eliášová, P.; Greer, H.; Zhou, W.; Seymour, V. R.; Dawson, D. M.; Ashbrook, S. E.; Pinar, A. B.; McCusker, L. B.; Opanasenko, M.; Čejka, J.; Morris, R. E. *Angew. Chem.* **2014**, *126*, 13426.
- (21) Burel, L.; Kasian, N.; Tuel, A. *Angew. Chem.* **2014**, *126*, 1384.
- (22) Xu, H.; Jiang, J.-g.; Yang, B.; Zhang, L.; He, M.; Wu, P. *Angew. Chem.* **2014**, *126*, 1379.
- (23) Corma, A.; Fornes, V.; Pergher, S. B.; Maesen, T. L. M.; Buglass, J. *Nature* **1998**, *396*, 353.
- (24) Roth, W.; Kresge, C.; Vartuli, J.; Leonowicz, M.; Fung, A.; McCullen, S. *Stud. Surf. Sci. Catal.* **1995**, *94*, 301.
- (25) Zhao, Z.; Zhang, W.; Ren, P.; Han, X.; Müller, U.; Yilmaz, B.; Feyen, M.; Gies, H.; Xiao, F.-S.; De Vos, D.; Tatsumi, T.; Bao, X. *Chem. Mater.* **2013**, *25*, 840.
- (26) Wu, P.; Ruan, J.; Wang, L.; Wu, L.; Wang, Y.; Liu, Y.; Fan, W.; He, M.; Terasaki, O.; Tatsumi, T. *J. Am. Chem. Soc.* **2008**, *130*, 8178.
- (27) Ikeda, T.; Kayamori, S.; Oumi, Y.; Mizukami, F. *J. Phys. Chem. C* **2010**, *114*, 3466.
- (28) Yilmaz, B.; Müller, U.; Feyen, M.; Zhang, H.; Xiao, F.-S.; De Baerdemaeker, T.; Tijsebaert, B.; Jacobs, P.; De Vos, D.; Zhang, W.; Bao, X.; Imai, H.; Tatsumi, T.; Gies, H. *Chem. Commun.* **2012**, *48*, 11549.
- (29) Roth, W. J.; Nachtigall, P.; Morris, R. E.; Čejka, J. *Chem. Rev.* **2014**, *114*, 4807.
- (30) Diaz, U.; Corma, A. *Dalton Trans.* **2014**, *43*, 10292.
- (31) Selvam, T.; Inayat, A.; Schwieger, W. *Dalton Trans.* **2014**, *43*, 10365.
- (32) Roth, W. J.; Gil, B.; Marszalek, B. *Catal. Today* **2014**, *227*, 9.
- (33) Marler, B.; Gies, H. *Eur. J. Mineral.* **2012**, *24*, 405.
- (34) Rodriguez, I.; Climent, M.; Iborra, S.; Fornes, V.; Corma, A. *J. Catal.* **2000**, *192*, 441.
- (35) Chal, R.; Gérardin, C.; Bulut, M.; Van Donk, S. *ChemCatChem.* **2011**, *3*, 67.
- (36) Groen, J. C.; Moulijn, J. A.; Pérez-Ramírez, J. *Microporous Mesoporous Mater.* **2005**, *87*, 153.
- (37) Verboekend, D.; Mitchell, S.; Milina, M.; Groen, J.; Pérez-Ramírez, J. *J. Phys. Chem. C* **2011**, *115*, 14193.
- (38) Pérez-Ramírez, J.; Abello, S.; Bonilla, A.; Groen, J. C. *Adv. Funct. Mater.* **2009**, *19*, 164.
- (39) Svelle, S.; Sommer, L.; Barbera, K.; Vennestrom, P. N. R.; Olsbye, U.; Lillerud, K. P.; Bordiga, S.; Pan, Y. H.; Beato, P. *Catal. Today* **2011**, *168*, 38.
- (40) Groen, J. C.; Peffer, L. A. A.; Moulijn, J. A.; Pérez-Ramírez, J. *Microporous Mesoporous Mater.* **2004**, *69*, 29.
- (41) Wei, X.; Smirniotis, P. G. *Microporous Mesoporous Mater.* **2006**, *97*, 97.
- (42) Holm, M. S.; Hansen, M. K.; Christensen, C. H. *Eur. J. Inorg. Chem.* **2009**, 1194.
- (43) Van Miltenburg, A.; Pawlesa, J.; Bouzga, A.; Žilková, N.; Čejka, J.; Stöcker, M. *Top. Catal.* **2009**, *52*, 1190.
- (44) Sommer, L.; Mores, D.; Svelle, S.; Stöcker, M.; Weckhuysen, B. M.; Olsbye, U. *Microporous Mesoporous Mater.* **2010**, *132*, 384.
- (45) Verboekend, D.; Groen, J. C.; Pérez-Ramírez, J. *Adv. Funct. Mater.* **2010**, *20*, 1441.
- (46) Verboekend, D.; Thomas, K.; Milina, M.; Mitchell, S.; Pérez-Ramírez, J.; Gilson, J.-P. *Catal. Sci. Technol.* **2011**, *1*, 1331.
- (47) Verboekend, D.; Keller, T. C.; Mitchell, S.; Pérez-Ramírez, J. *Adv. Funct. Mater.* **2013**, *23*, 1923.
- (48) Verboekend, D.; Keller, T. C.; Milina, M.; Hauert, R.; Pérez-Ramírez, J. *Chem. Mater.* **2013**, *25*, 1947.
- (49) Biemelt, T.; Selzer, C.; Schmidt, F.; Mondin, G.; Seifert, A.; Pinkert, K.; Spange, S.; Gemming, T.; Kaskel, S. *Microporous Mesoporous Mater.* **2014**, *187*, 114.
- (50) Góra-Marek, K.; Tarach, K.; Choi, M. *J. Phys. Chem. C* **2014**, *118*, 12266.
- (51) Ogura, M.; Shinomiya, S.-y.; Tateno, J.; Nara, Y.; Nomura, M.; Kikuchi, E.; Matsukata, M. *Appl. Catal., A* **2001**, *219*, 33.
- (52) Groen, J. C.; Peffer, L. A. A.; Moulijn, J. A.; Pérez-Ramírez, J. *Chem.—Eur. J.* **2005**, *11*, 4983.
- (53) Verboekend, D.; Pérez-Ramírez, J. *Chem.—Eur. J.* **2011**, *17*, 1137.
- (54) Gies, H.; Müller, U.; Yilmaz, B.; Feyen, M.; Tatsumi, T.; Imai, H.; Zhang, H.; Xie, B.; Xiao, F. S.; Bao, X.; Zhang, W.; De Baerdemaeker, T.; De Vos, D. *Chem. Mater.* **2012**, *24*, 1536.
- (55) De Baerdemaeker, T.; Gies, H.; Yilmaz, B.; Müller, U.; Feyen, M.; Xiao, F.-S.; Zhang, W.; Yokoi, T.; Bao, X.; De Vos, D. *E. J. Mater. Chem. A* **2014**, *2*, 9709.
- (56) Emeis, C. *J. Catal.* **1993**, *141*, 347.
- (57) Klinowski, J.; Thomas, J. M.; Fyfe, C. A.; Gobbi, G. C. *Nature* **1982**, *296*, 533.
- (58) Jiang, J.-G.; Jia, L.; Yang, B.; Xu, H.; Wu, P. *Chem. Mater.* **2013**, *25*, 4710.
- (59) Roth, W. J.; Kresge, C. T. *Microporous Mesoporous Mater.* **2011**, *144*, 158.
- (60) Yang, B.; Jiang, J.-g.; Xu, H.; Ji, P.; Wu, P. *Microporous Mesoporous Mater.* **2015**, *203*, 54.
- (61) De Baerdemaeker, T.; Vandebroeck, W.; Gies, H.; Yilmaz, B.; Müller, U.; Feyen, M.; De Vos, D. *Catal. Today* **2014**, *235*, 169.
- (62) Verboekend, D.; Perez-Ramirez, J. *Catal. Sci. Technol.* **2011**, *1*, 879.
- (63) Bjørgen, M.; Joensen, F.; Spangsberg Holm, M.; Olsbye, U.; Lillerud, K.-P.; Svelle, S. *Appl. Catal., A* **2008**, *345*, 43.
- (64) Groen, J. C.; Abelló, S.; Villaescusa, L. A.; Pérez-Ramírez, J. *Microporous Mesoporous Mater.* **2008**, *114*, 93.